Comparison of the performance of falling film and bubble absorbers for air-cooled absorption systems ☆

J. Castro, C. Oliet, I. Rodríguez, A. Oliva *

Centre Tecnològic de Transferència de Calor (CTTC), Universitat Politècnica de Catalunya (UPC), ETSEIAT, Colom 11, E08222 Terrassa (Barcelona), Spain

ABSTRACT

Small capacity, air-cooled NH_3–H_2O absorption systems are becoming more attractive in applications where the input energy can be obtained for free (e.g., solar energy, exhaust gases of engines), due to the increasing price of the primary energy. One of the main difficulties for a wider use of absorption machines is the necessary high initial investment. For this reason, the development of air-cooled systems could be an important achievement for low capacity applications. In this work, two types of air-cooled absorber have been modelled: (i) falling film flow; (ii) bubble flow. The two models have been validated with experimental data obtained from a developed testing device and published numerical results of other authors from another model. The agreement is acceptable for both cases. Finally, a parametric study has been done for air-conditioning and refrigeration in a mobile application taking advantage of the exhaust gases of the engine. In both cases, the performance of the bubble absorber has been higher.

© 2008 Elsevier Masson SAS. All rights reserved.

1. Introduction

The increasing price of the primary energy makes absorption refrigeration technology more attractive. The main obstacle that makes difficult its extended use is the high initial investment necessary. This problem is especially important for low capacity machines, e.g., domestic or mobile applications. As a consequence, most available technology is only suitable for large dimension installations where the extra cost of the absorption system could be assumed. In order to develop low cost absorption machines of small capacity, air-cooling of the absorber and condenser is an important characteristic to avoid the cooling tower and, by consequence, to reduce the price of the whole installation [1].

NH_3–H_2O as fluid pair makes the use of the absorption machine more universal, as chiller in summer and as heat pump in winter. Recent developments in NH_3–H_2O systems make them competitive in terms of performance with respect to H_2O–LiBr ones [2], even in air-conditioning applications. There is a big potential market for absorption technology for air-conditioning, in household

(e.g., solar cooling installations in the Mediterranean area) and mobile applications (taking advantage of the exhaust gases of the engine) and, on the other hand, refrigeration (e.g., food, chemical and pharmaceutical industries). According to the author's knowledge, there is not commercial solution available for the case of mobile applications. Most of the research work in absorption technology has been focused on air-conditioning applications [3–5]. Only few researchers focused the attention on refrigeration applications, where the pair refrigerant–absorbent NH_3–H_2O is the most suitable one [6–8]. Koehler et al. [7] suggest that most of the schemes proposed are not adequate from a thermodynamic or manufacturing point of view.

The high price of the absorption chillers is related with the complexity of the system and the size of the heat exchangers. The absorber usually is the largest element of absorption machines due to its low heat and mass transfer coefficients, and this fact determines the final design of the whole system. For this reason, the development of a numerical tool is interesting for the design and optimisation of the air-cooled absorbers. Typically, there are two types of absorber suitable for the pair refrigerant–absorbent NH_3–H_2O: falling film and bubble type. Absorption processes in NH_3–H_2O systems have been less studied than in H_2O–LiBr systems, and moreover most of them are referred to water-cooled absorbers of horizontal tubes [9,10]. However, due to the increasing interest of generator-absorber heat exchange cycles, there is a renewal of the

Nomenclature

A	heat exchange area	m^2
a	thermal diffusivity	$m^2 s^{-1}$
c	concentration % weight	
c_p	heat capacity at constant pressure	$J kg^{-1} K^{-1}$
D	Fick's law mass diffusivity coefficient	$m^2 s^{-1}$
d	diameter	m
e	thickness of the mass transfer slice in the bubble	m
h	enthalpy	$J kg^{-1}$
i	position of control volume in x direction	
j	position of control volume in y direction	
K	mass transfer coefficient	$kg s^{-1} m^{-2}$
k	position of control volume in z direction	
L	length of a side of the air–liquid heat exchanger	m
$\dot{m}$	mass flow	$kg s^{-1}$
N_k	number of control volumes in k direction ($k : x, y, z$)	
n	normal direction to the liquid–vapour interface	
P	perimeter	m
p	pressure	$N m^{-2}$
$\dot{Q}$	heat dissipated	W
Sh	Sherwood number	
r	inner radius of the tube	m
T	temperature	K
u	component velocity of the falling liquid parallel to wall	$m s^{-1}$
V	absolute velocity	$m s^{-1}$
v	component velocity of the falling liquid orthogonal wall	$m s^{-1}$
x	direction parallel to wall	m
y	direction orthogonal to wall	m
z	direction parallel to wind direction	m

Greek symbols

α	heat transfer coefficient	$W m^{-2} K^{-1}$
δ	falling film thickness	m
ϵ	void fraction	
Γ	mass flow per unit length	$kg s^{-1} m^{-1}$
ν	kinematic viscosity	$m^2 s^{-1}$
ρ	density	$kg m^{-3}$
θ	angle respect to gravity	rad
ζ	static contact angle	rad

Subscripts

a	ammonia
abs	absorption
air	air
b	bulk
bub	related to bubble
cal	calculated
eq	equilibrium
exp	experimental
i	interface
in	inlet
l	liquid
mass	related to mass
max	maximum
out	outlet
sol	solution
sup	superficial
v	vapour
W	related to wall
w	water
wet	wetted

Table 1
Characteristics comparison between falling film and bubble type absorbers [15].

Type of absorber	Falling film	Bubble
Interfacial area	Small	Large
Heat transfer area	Similar to interfacial area	Smaller than interfacial area
Mixing	Poor	Excellent
Wettability	Critical	Excellent
Liquid distributor	Yes, liquid management	No
Vapour distributor	No	Yes, orifice of vapour management
Flooding	Yes for counter/No for co-current	Yes
Heat and mass transfer	Liquid and vapour	Liquid and vapour
Compactness	Good	Excellent

interest of absorption processes in vertical falling films [11,12] or bubble absorbers [13,14]. The advantages and disadvantages of the two types of absorber are summarised in Table 1 [15]. Moreover, falling film absorbers are more sensitive to vibrations and changes in the verticality than bubble absorbers (e.g., mobile applications). In this work, the two type of air-cooled absorbers are modelled. The absorption processes calculation subroutines of are validated and finally, a parametric study comparing the two absorbers is carried out.

2. Mathematical formulation

The absorber modelled is a battery of vertical finned tubes. In the case of falling absorption, the liquid flows down in the in-ner part of the tube that is directly cooled by air. The liquid is distributed at the top of the tubes, forming the falling film. The vapour is also introduced in the top part of the tube. In bubble absorption, the liquid and vapour are introduced at the bottom part of each tube. The bubbles formed flow up and also the liquid goes upward, therefore, having cocurrent flow.

2.1. Fin and tube compact heat exchanger

Fig. 1 shows details of the modelling of the heat exchanger. For the analysis of the air-side and solid parts (tubes and fins), a fin-and-tube heat exchanger design code written in C++ platform has been used [16–18]. This code has been the main tool on the design and optimisation of the air-cooled absorbers. In order to keep within reasonable limits the CPU time consumption, the mathematical formulation requires the knowledge of some empirical information such as local heat transfer coefficients, and friction factors. This empirical information does not depend on a specific heat exchanger but the kind of heat transfer surfaces (in this case of study wavy fin), and local flow structure [19]. For the air flow, the equations of conservation of energy and momentum are solved in each control volume (CV) in which the whole heat exchanger is divided. The energy equation in the solid is solved taking into account the axial heat transfer in the tubes and an analytical expression for calculating the performance of the fins. The inner flow is modelled by a specific subroutine, for falling film or bubble absorption.
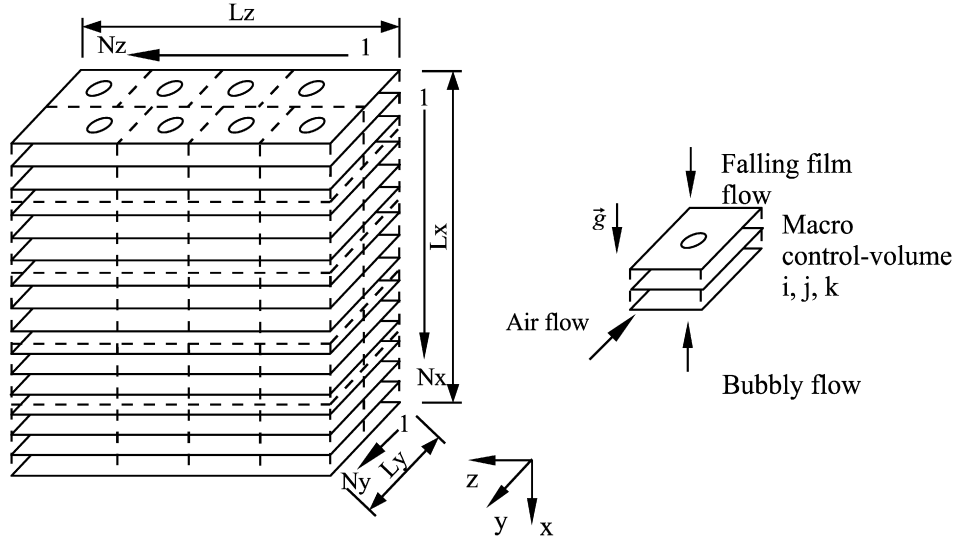
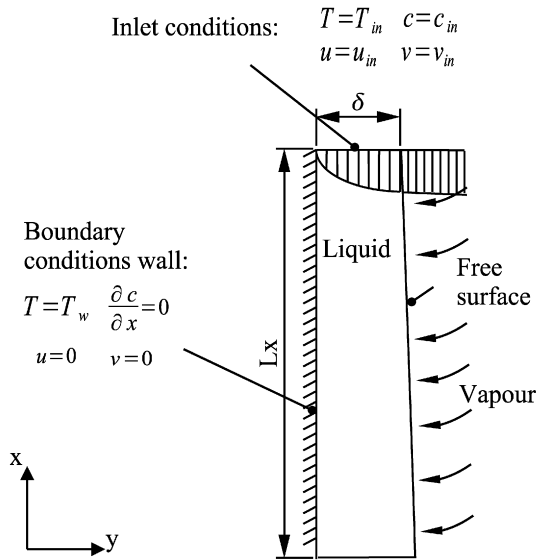**Fig. 1.** Scheme of discretisation of air–liquid compact heat exchangers.

Fig. 2. Falling film boundary conditions.

2.2. Falling film absorption

The absorption process in the falling liquid film is produced over a smooth surface. Moreover, there is no presence of any additive that could produce additional movements in the liquid film, therefore boundary layer hypotheses for the governing equations are assumed. On the other hand, the mass flow is so low that does not assure a complete area wetted of the vertical surface. By consequence, a correction for considering this effect has been implemented. This model was already presented in [20] and [21] for NH$_3$–H$_2$O and H$_2$O–LiBr air-cooled absorbers, respectively. The following hypotheses are assumed:

- Steady state flow.
- Axisymmetric geometry.
- Physical properties variable only in the flow direction.
- The heat and mass transfer coefficients towards the vapour phase are calculated by means of the penetration theory [22].
- There is no shear stress at the interface.
- Thermodynamic equilibrium at the interface.
- The flow is laminar and incompressible.

- The diffusion terms are negligible in the flow direction.
- The convection terms are negligible in the direction orthogonal to the flow.
- The pressure gradients are negligible.
- The initial velocity considered corresponds to fully developed laminar flow regime.
- Dufour and Soret effects have not been considered.
- The wettability model considered calculates the fraction of wetted area, readapting the mass flow per unit length to the new area. It does not take into account any particular velocity profile of the falling rivulets.

Under the above hypothesis, these are the governing equations:

$$\frac{\partial u}{\partial x} + \frac{\partial v}{\partial y} = 0 \tag{1}$$

$$u\frac{\partial u}{\partial x} + v\frac{\partial u}{\partial y} = g\cos(\theta) + \nu\frac{\partial^2 u}{\partial y^2} \tag{2}$$

$$u\frac{\partial T}{\partial x} + v\frac{\partial T}{\partial y} = a\frac{\partial^2 T}{\partial y^2} \tag{3}$$

$$u\frac{\partial c}{\partial x} + v\frac{\partial c}{\partial y} = D\frac{\partial^2 c}{\partial y^2} \tag{4}$$

The equations are: continuity (1), momentum conservation (2), energy conservation (3) and NH$_3$ conservation (4). The partial differential equations system is solved by means of a change of coordinates taking into account the variation of the thickness of the falling film. Due to the parabolic structure of the system of equations, the flow is solved in a step-by-step procedure. This model predicts absorption phenomena over smooth surfaces of H$_2$O–LiBr systems reasonably [23], in case that a complete wetted area is achieved. The boundary conditions at the interface are:

$$T_{\text{eq}} = f(p, c_{\text{eq},l}), \qquad c_{\text{eq},v} = f(p, c_{\text{eq},l}) \tag{5}$$

$$\lambda_l\frac{\partial T}{\partial y} + \alpha_v(T_i - T_{v,b}) = (h_{\text{abs},a}d\dot{m}_a + h_{\text{abs},w}d\dot{m}_w)/dA_i \tag{6}$$

$$\frac{\partial u}{\partial n} = 0 \tag{7}$$

Eq. (5) describes thermodynamic equilibrium at the interface [24], Eq. (6) is a heat balance at the interface that relates the incoming heat transfer, sensible and latent. Eq. (7) indicates no shear

stress at the interface. The mass absorbed of NH_3 and H_2O is calculated by means of the following expressions:

$$dm_a = dm_{l,a} = -dm_{v,a}$$

$$dm_w = dm_{l,w} = -dm_{v,w} \tag{8}$$

$$dm_l = -dm_v = dm_{l,a} + dm_{l,w} = -dm_{v,a} - dm_{v,w} \tag{9}$$

$$dm_{l,a} = dA_i\left(-\rho_l D_l \frac{\partial c_{l,a}}{\partial y}\right) + c_{i,l,a}dm_l \tag{10}$$

$$dm_{l,w} = dA_i\left(-\rho_l D_l \frac{\partial c_{l,w}}{\partial y}\right) + c_{i,l,w}dm_l \tag{11}$$

$$dm_{v,a} = dA_i\left(-\rho_v D_v \frac{\partial c_{v,a}}{\partial y}\right) + c_{i,v,a}dm_v \tag{12}$$

$$dm_{v,w} = dA_i\left(-\rho_v D_v \frac{\partial c_{v,w}}{\partial y}\right) + c_{i,v,w}dm_v \tag{13}$$

Where:

$$dA_i = P_{\text{wet}} dx \tag{14}$$

Eq. (10) expresses by means of the Fick's law [22] for a moving fluid the mass flow of NH_3 from the point of view of the liquid. Eq. (11) is the same expression applied to H_2O, and Eqs. (12) and (13) are the analogous expressions applied from the point of view of the vapour. These four equations can be reduced to two taking into account that:

$$c_{l,a} = 1 - c_{l,w} \tag{15}$$

$$c_{v,a} = 1 - c_{v,w} \tag{16}$$

thus,

$$-\rho_l D_l \frac{\partial c_{l,a}}{\partial y} = \rho_l D_l \frac{\partial c_{l,w}}{\partial y} \tag{17}$$

$$-\rho_v D_v \frac{\partial c_{v,a}}{\partial y} = \rho_v D_v \frac{\partial c_{v,w}}{\partial y} \tag{18}$$

Therefore, there are two equations and two unknowns (dm_a and dm_w). However, it is necessary to calculate the diffusive mass fluxes (in the liquid and in the vapour) to know the total mass fluxes. In the liquid, the diffusive mass flux is calculated by means of the resolution of the partial differential equations system (Eqs. (1)–(4)). Then, the concentration derivative is calculated by finite difference of the concentration map resulting from the resolution of the deduced algebraic system of equations. From this diffusive mass flux, a mass transfer coefficient can be defined from the liquid side:

$$K_l = -\frac{\rho_l \frac{\partial c_l}{\partial y}}{(c_{l,a,i} - c_{l,a,b})} \tag{19}$$

A diffusive mass flow is also considered in the vapour side, therefore, a resistance to mass transfer. As in the case of the liquid side, a coefficient of mass transfer with respect the vapour phase is also defined in the same way. This coefficient is calculated from the penetration theory [22], that assumes a constant value of the vertical velocity in all the zone where the NH_3 concentration derivative with respect y-coordinate is different from zero. Therefore, a low penetration of the boundary layer of the mass species equation in the vapour phase is considered:

$$K_v = \rho_v\sqrt{\frac{D_v v_{\max}}{\pi y}} \tag{20}$$

Arranging the previous equations, the following expressions can be deduced for calculating NH_3 mass flux at the interface:

$$dm_a = dA_i\left(\frac{K_v(c_{v,a,b} - c_{v,a,i}) + \frac{c_{v,a,b}}{c_{l,a,b}}K_l(c_{l,a,b} - c_{l,a,i})}{\left(1 - \frac{c_{v,a,b}}{c_{l,a,b}}\right)}\right) \tag{21}$$

And the mass flux of H_2O at the interface:

$$dm_w = dA_i\left(\frac{K_v(c_{v,a,i} - c_{v,a,b}) + \frac{1 - c_{v,a,b}}{1 - c_{l,a,b}}K_l(c_{l,a,i} - c_{l,a,b})}{\frac{c_{v,a,b} - c_{l,a,b}}{1 - c_{l,a,b}}}\right) \tag{22}$$

Heat transfer in the vapour side of the falling film is evaluated by the calculation of a heat transfer coefficient by analogy with the mass species equation:

$$\alpha_v = \rho_v c_{p,v}\sqrt{\frac{a_v u_{\max}}{\pi y}} \tag{23}$$

As commented above, in real falling films a complete wetted area is not assured under a certain value of mass flow per unit length. In order to consider non-wettability effects, the model of Mikielewicz et al. [25] has been implemented. This model assumes a circular profile of the rivulets and proposes a formula for calculating the fraction of wetted area, as a function of the contact angle and mass flow per unit length, with the criteria of minimum energy. In this work, this fraction of wetted area is then introduced as a factor that reduces the heat and mass transfer with respect to the case of a complete wetted area, without taking into account any particular profile. Consequently, the mass flow rate per unit length is corrected to the new wetted tube perimeter. For calculating the minimum flow rate to achieve a complete wetted area, the criterion given by Hobler et al. has been considered. This criterion is also reported in [25] and agrees better with the experimental data than the criterion deduced from Mikielewicz model:

$$P_{\text{wet}} = 2\pi r f(\zeta, \Gamma) \tag{24}$$

Where:

$$\Gamma = \frac{m_l}{2\pi r} \tag{25}$$

2.3. Bubble absorption

In the case of bubble absorption, a similar model to Herbine and Pérez-Blanco [13] and Lee et al. [14] has been developed. The main similarities are concerning the fluid dynamics, but there are important differences with respect to the heat and mass transfer calculations [26]. The hypotheses assumed in the model are:

- Steady state flow.
- One-dimensional process along the tube length.
- Spherical vapour bubbles.
- Bubble break-up and coalescence not considered.
- Relations of bubble temperature, pressure and volume as ideal gas.
- Mass transfer flux constant on the entire surface of the bubble.
- Linear profile of temperatures and concentrations inside the bubble (heat and mass transfer coefficients at the vapour side).
- No direct heat transfer between the vapour and the wall.

For solving the conservation equations (continuity, momentum, energy and mass species) of the bubble absorption process, the whole domain (tube) is discretised along its coordinate parallel to the main direction flow (x). Fig. 3 shows the scheme of a control volume. As in the case of falling film absorption, the mass flow through the interface of ammonia and water are calculated according to Eqs. (21) and (22), respectively. In the case of bubble absorption the interfacial area (A_i) in the control volume is calculated according to the values of bubble diameter, d_{bub}, and bubble

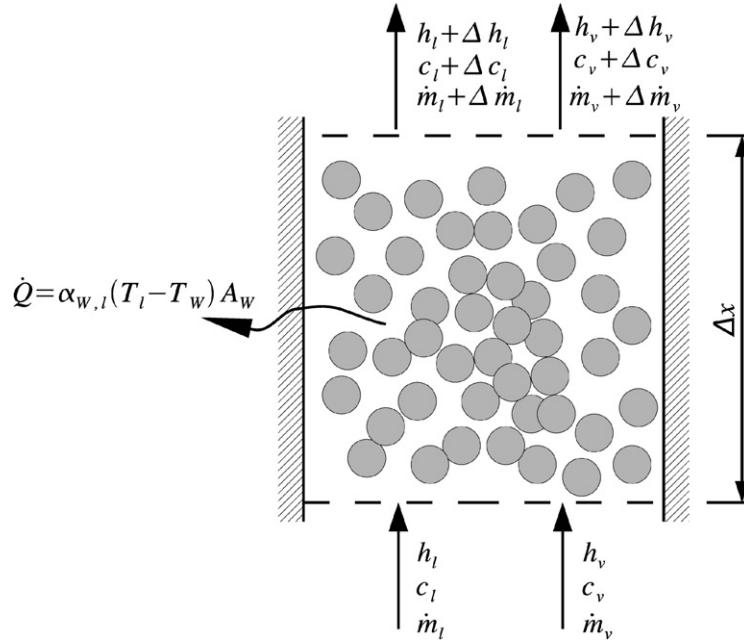$$\dot{Q} = \alpha_{W,l}(T_l - T_w)A_w$$

Fig. 3. Scheme of the control volume in bubbly flow.

absolute velocity, V_{bub}, which are determined from empirical expressions [27]:

$$dA_i = \frac{\dot{m}_v}{V_{\text{bub}}\rho_v \frac{1}{6}d_{\text{bub}}}dx \tag{26}$$

The mass transfer coefficient for the liquid side is calculated from the following expression where the Sherwood number is calculated from empirical correlations [27]:

$$K_l = \rho_l Sh_l D_l / d_{\text{bub}} \tag{27}$$

As commented above, it is assumed a linear profile of NH_3 concentration in the bubble. This leads to:

$$K_v = \rho_v D_v / e \tag{28}$$

where e is the thickness of the slices of the bubble with concentration different from the initial.

The new concentrations at the liquid and vapour phases are calculated according to the mass fluxes:

$$dc_{l,a} = \left[\frac{\dot{m}_l c_{l,a} + \dot{m}_v c_{v,a} - (\dot{m}_v + d\dot{m}_v)(c_{v,a} + dc_{v,a})}{\dot{m}_l + d\dot{m}_l}\right] - c_{l,a} \tag{29}$$

$$dc_{v,a} = \left[\frac{\dot{m}_v c_{v,a} - d\dot{m}_{v,a}}{(\dot{m}_v + d\dot{m}_v)}\right] - c_{v,a} \tag{30}$$

Concerning the heat transfer, the variations of enthalpy at the liquid and vapour phases are calculated by means of energy balances at each phase, respectively:

$$dh_l = \frac{\alpha_{W,l}A_W(T_W - T_l) + d\dot{m}_{l,a}h_{l,a,i} + d\dot{m}_{l,w}h_{l,w,i}}{\dot{m}_l + d\dot{m}_l}$$
$$+ \frac{\alpha_{\text{bub},l}A_i(T_i - T_l) - d\dot{m}_l h_l}{\dot{m}_l + d\dot{m}_l} \tag{31}$$

$$dh_v = \frac{d\dot{m}_{v,a}h_{v,a,i} + d\dot{m}_{v,w}h_{v,w,i} + \alpha_{\text{bub},v}A_i(T_i - T_l) - d\dot{m}_v h_v}{\dot{m}_v + d\dot{m}_v} \tag{32}$$

A_W is the area of the control volume boundary to the wall. The heat transfer coefficients at the interface $\alpha_{\text{bub},l}$ and $\alpha_{\text{bub},v}$ are calculated by analogy with respect mass transfer. The heat transfer

coefficient towards the wall $\alpha_{W,l}$ is calculated according the following expression [13], where α is the heat transfer coefficient in single phase:

$$\alpha_{W,l} = \alpha(1 - \epsilon)^{-0.8} \tag{33}$$

The conditions at the interface are calculated assuming the equilibrium relations [24] (see Eq. (5)) and heat transfer balance:

$$T_i = \frac{d\dot{m}_{l,a}h_{\text{abs}} + d\dot{m}_{l,w}h_{\text{abs}} + A_i(\alpha_{\text{bub},l}T_l + \alpha_{\text{bub},v}T_v)}{A_i(\alpha_{\text{bub},l} + \alpha_{\text{bub},v})} \tag{34}$$

3. Validation of the models

In this section the models implemented for both falling film and bubble absorption are validated comparing the numerical results with experimental data.

3.1. Falling film absorber

In order to validate the model of falling film absorber, an experimental device has been built. The absorber tested consists on a battery of tubes with plain fins and staggered tube arrangement. The material is carbon steel for the tubes and fins. The rest of the unit is made of stainless steel. The heat exchanger is placed in a wind tunnel where is cooled by a variable speed fan. The absorber has 4 tube rows in air flow direction (N_y), with a separation of 56.66 mm, 6 tubes in the direction orthogonal (N_z), with a separation of 66.66 mm, the tube length is 1.2 m with an outer diameter of 22 mm (1.3 mm of tube thickness) and the fin pitch is 5 mm. The tube arrangement is staggered.

Fig. 4 shows the connections between elements. The operation of the experimental test device of the absorber is as follows: starting from the generator shell, the pressure difference drives the solution towards the absorber (1–1′). The mass flow, density, and temperature are measured. The generator is driven by hot oil and by consequence the NH_3 vapour is produced and the solution is concentrated. This continuous production of NH_3 vapour maintains the absorption pressure (2–2′). Then, the NH_3 vapour arrives to a liquid separator, to split the possible liquid produced due to condensations. The liquid goes to solution line (3–3′) and the vapour
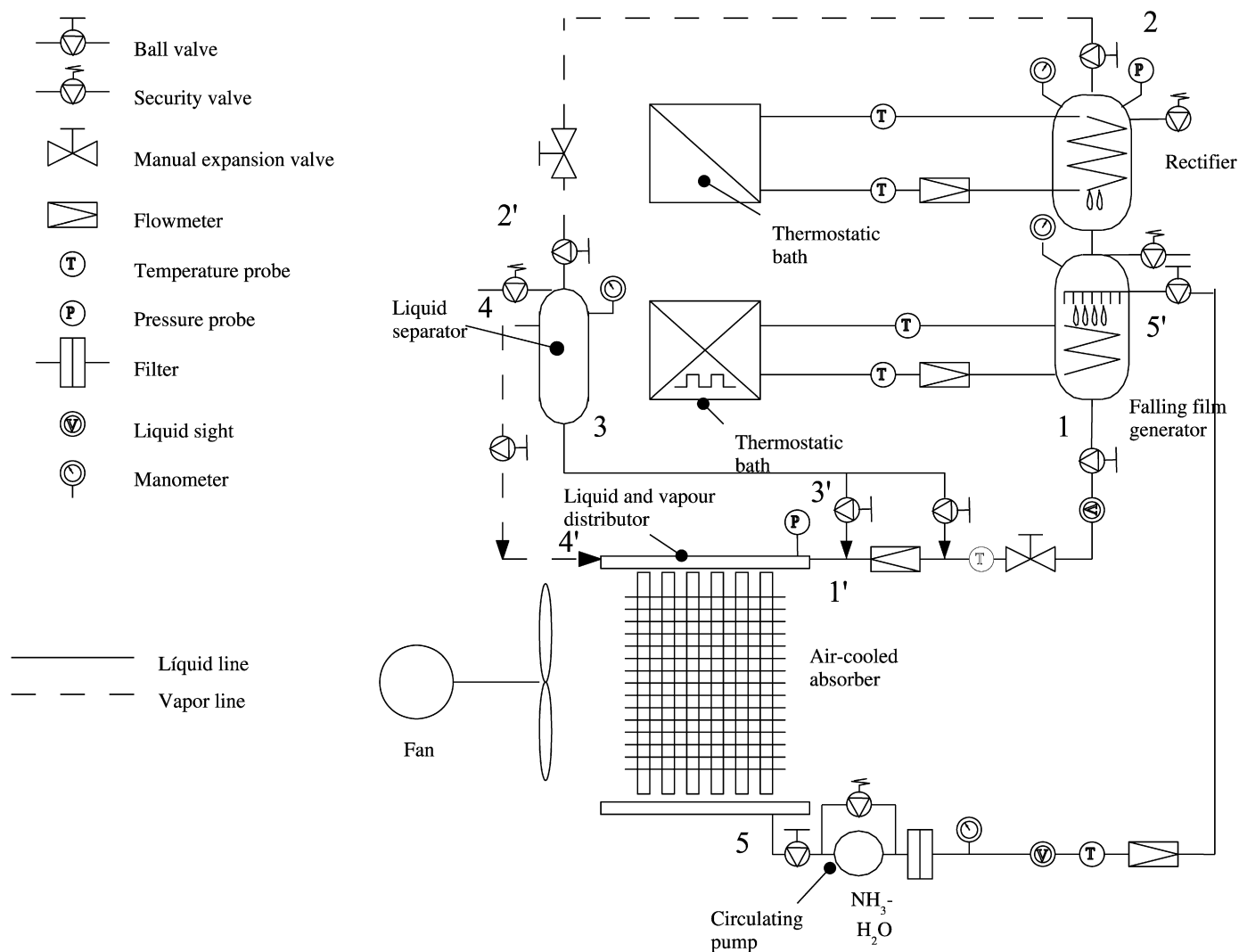
Fig. 4. Scheme of the falling film absorber experimental test device.

to the absorber distributor (4–4′). When the concentrated solution arrives to the absorber, it is fairly distributed in all the absorber tubes (1′). The diluted solution goes down to the pump. Finally, this pump drives the solution again to the generator shell (5–5′) and the mass flow and density are also measured and the loop starts again.

Fig. 5 shows a picture of the whole experiment with the absorber in the central part. In the upper part of the absorber, there is a solution falling film distributor. Metallic meshes at the top of each tube guaranteed a fair distribution between tubes and also produce the falling film formation.

In order to have a more accurate measurement of the heat dissipated by the absorber on the air side, several points of temperature measurement with the same influence area have been taken in the inlet (2 width × 2 height points) and outlet section (2 × 4). In order to measure the air velocity, an array of 7 × 11 points uniformly distributed have been taken into account. The measurement has been carried with a hot wire anemometer with values averaged in time.

Several comparisons have been performed between the experimental results of the air-cooled absorber and the numerical ones with the model developed. Table 2 shows the input conditions and output values of the different tests. The values shown in each column are, respectively: number of test, absorption pressure, air mass flow, inlet air temperature, volumetric flow of solution, in-

let solution temperature and inlet solution concentration, outlet air temperature, experimental and calculated, outlet solution temperature, experimental and calculated, outlet concentration, experimental and calculated. The vapour has been considered as pure NH_3. The value of contact angle considered between the NH_3–H_2O solution and the carbon steel has been considered as 89° (close to neutral behaviour), value similar to the typical one of H_2O in carbon steel.

It can be observed that in general, for the solution flow, the model overpredicts the change of concentration and the change of temperature. Fig. 6 compares the predicted heat dissipated with the measured in the solution stream (a), and in the air stream (b).

The agreement between the experimental and numerical results are quite independent of the internal and external mass flows. There is a reasonable agreement between the numerical results given by the model developed and the experimental ones, especially with the experimental values from the air circuit, in most of the cases under 15%. The main reason for the discrepancies was the low temperature jump of the air stream, that leads to significative errors. The main discrepancies are found when the comparison is performed with the values from the solution circuit. These discrepancies are due to measurement errors in the density of the NH_3–H_2O solution and, by consequence, of NH_3 concentration in the primary circuits because of presence of vapour bubbles. The

Fig. 5. Falling film absorber experimental test device.

calculations indicate a poor percentage of wetted area (less than 15%) due to the high value of the contact angle between the solution and the steel considered.

3.2. Bubble absorber

For validating the model developed, the numerical results given by Herbine and Pérez-Blanco [13] of a water-cooled, double-pipe, bubble absorber, have been used as benchmark. Table 3 summarises the geometry and working conditions of the case. The bubbly flow goes in the inner tube and the coolant flow through the annulus. Although the heat exchanger is in counter flow between the bubbly flow and the coolant, the flow is cocurrent between liquid and vapour in the bubble absorption process.
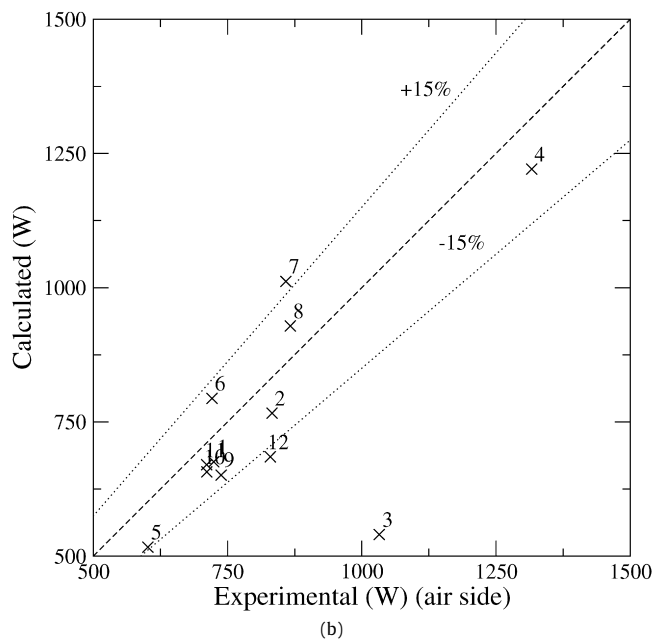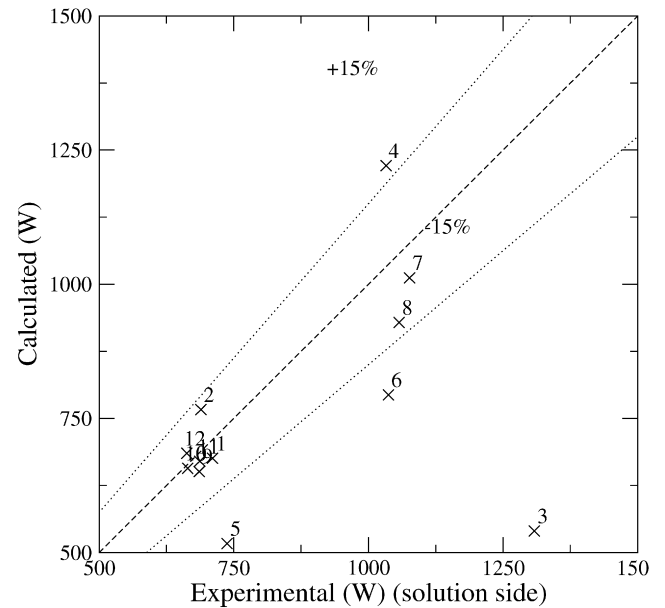

Fig. 6. Comparison of the heat dissipated (experimental values of heat transfer from primary (a) and secondary (b) circuits). The conditions of the experimentation are in Table 2.

Table 2
Data of the different tests.

Test n°	Absorber pressure (kPa)	Air flow (kg s^{-1})	Air T_{in} (°C)	Solution flow (m^3 s^{-1}·10^5)	Solution T_{in} (°C)	Solution c_{in} (%w NH$_3$)	Air $T_{out,exp}$ (°C)	Air $T_{out,cal}$ (°C)	Solution $T_{out,exp}$ (°C)	Solution $T_{out,cal}$ (°C)	Solution $c_{out,exp}$ (%w NH$_3$)	Solution $c_{out,cal}$ (%w NH$_3$)
1	94.16	0.60	29.39	5.25	35.29	22.05	30.59	30.50	32.44	31.58	22.62	23.05
2	94.23	0.60	28.89	5.32	35.37	21.91	30.28	30.16	32.29	31.46	22.55	22.95
3	86.20	1.29	30.25	5.13	35.35	21.94	31.05	30.67	32.45	31.13	22.78	22.79
4	95.14	1.30	27.23	5.06	35.68	21.44	28.23	28.15	30.45	30.69	22.78	22.64
5	90.97	0.60	26.64	2.63	34.89	21.41	27.86	27.71	28.56	29.70	22.31	22.58
6	89.66	0.60	26.64	2.63	34.26	21.49	27.82	27.72	28.61	29.58	22.68	22.62
7	87.85	1.30	26.71	2.63	33.91	21.46	27.25	27.21	28.00	29.10	22.26	22.59
8	91.67	1.30	27.03	2.63	34.99	21.44	27.66	27.55	28.52	29.66	22.31	22.63
9	109.10	0.59	30.90	1.34	42.90	20.91	31.90	31.76	31.81	33.95	22.50	22.36
10	139.10	0.59	29.53	1.39	48.97	19.90	30.96	31.20	31.05	35.86	22.30	22.16
11	117.46	0.60	26.50	1.34	42.74	20.68	27.69	27.82	27.91	31.89	22.37	22.52
12	136.17	0.60	28.67	1.36	47.60	20.07	30.12	30.21	30.19	34.65	22.42	22.81

Table 3
Geometry and working conditions of the double-pipe, bubble absorber.

Geometry	Units		Input conditions	Units	
Inner tube, outer diameter	(m)	12.7×10^{-3}	Solution mass flow	(g/s)	0.5020
Inner tube, thickness	(m)	0.9×10^{-3}	Vapour mass flow	(g/s)	0.0058
Outer tube, outer diameter	(m)	25.4×10^{-3}	Coolant mass flow	(g/s)	1.2545
Outer tube, thickness	(m)	1.65×10^{-3}	Solution temperature	(°C)	126.7
Vapour injector holes diameter	(m)	0.90×10^{-3}	Vapour temperature	(°C)	40.0
Tubes length	(m)	7.62×10^{-1}	Coolant temperature	(°C)	106.7
			Solution concentration	(%w NH$_3$)	7.3
			Vapour concentration	(%w NH$_3$)	99.4
			Pressure	(kPa)	501.8

Fig. 7 shows the comparison between the results of the model developed and the numerical results provided by Herbine and Pérez-Blanco [13]. In the comparison of the NH$_3$ and H$_2$O mass flow absorbed by the liquid in a single bubble can be observed that the two models provide similar results from a qualitative point of view. However, the mass flow rates calculated by the model developed in this work are in general higher, except for the case of ammonia at the beginning of the absorption process. The discrepancies can be explained by the different manner of calculation of the mass absorbed, respect the model of Herbine and Pérez-Blanco. On the other hand, in the case of the temperature profiles of the liquid solution and the coolant the quantitative agreement is better than in the case of the mass absorbed. The discrepancies are due mainly to the underestimation of the NH$_3$ absorbed at the beginning of the process. The higher value of mass absorbed calculated by the model of Herbine and Pérez-Blanco in this zone implies higher solution temperatures and higher heat transfer rates to the coolant.

4. Parametric studies

In order to study the performance of the two types of air-cooled absorber a parametric study has been carried out. Three absorbers with the same number of tubes but different arrangement have been tested numerically. The parametric studies have been performed under two characteristic input conditions: air-conditioning [5] and refrigeration [26] for a case of mobile application taking advantage of the exhaust gases. Table 4 summarises the geometry and working conditions. The parametric study is based on the variation of the solution and air streams for the three absorbers studied, under air-conditioning and refrigeration applications, and for the two types of flow, falling film and bubble.

4.1. Influence of the flow type

In Fig. 8 the heat dissipated vs. the mass flow in the solution and air stream is depicted. It can be observed that there are no important differences from a qualitative point of view for the two type of working conditions, air-conditioning and refrigeration. For these particular tested cases, under air-conditioning conditions the heat dissipated has been higher than in refrigeration conditions, but the relative differences between the bubble and falling film absorber in refrigeration mode are more evident.

In order to clarify the information, Fig. 9 depicts with more detail the data of Fig. 8 for air-conditioning conditions. In these plots can be observed the stronger influence in the heat dissipated of the primary mass flow (solution) for low $\dot{m}_{sol}$. At high $\dot{m}_{sol}$ rates, airside is the dominant thermal resistance. For both types of absorber, there is a value of the primary mass flow in which the maximum performance is reached and, after that, it has no sense to increase the solution pumped. However, there are differences between the two types of absorber, because this
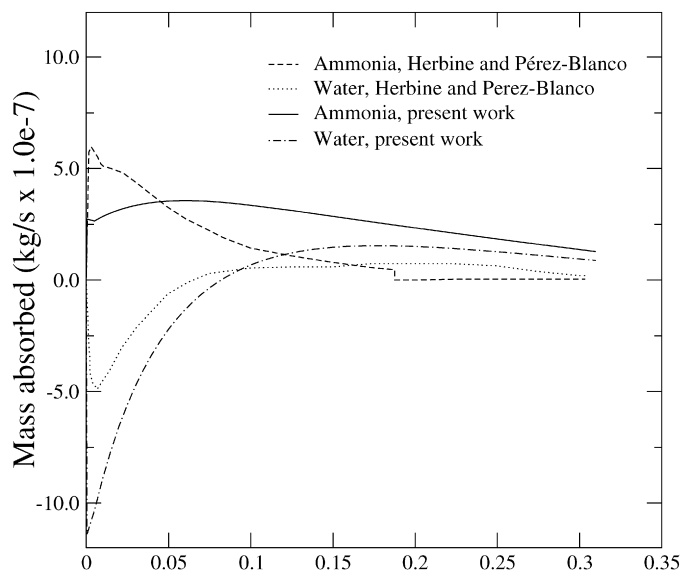

(a)
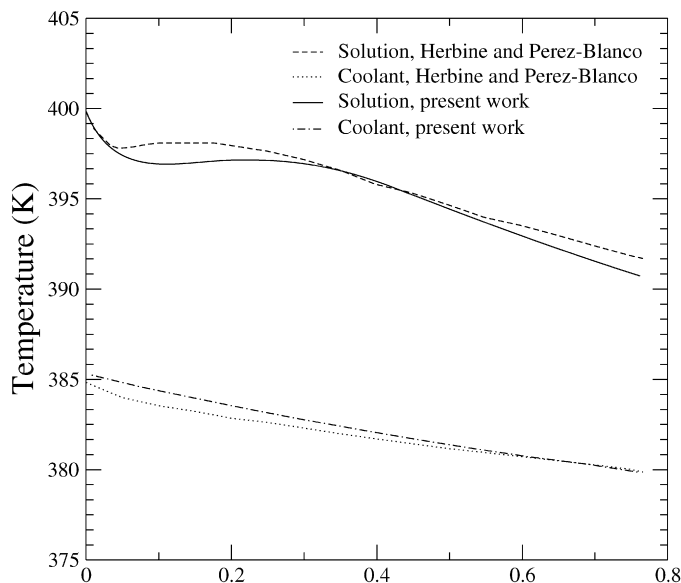
(b)

Fig. 7. Comparison of the mass absorbed in a bubble (a) and the temperature profiles (b).

Table 4
Geometry and working conditions of the air-cooled absorber.

Geometry	Units		Input conditions	Units	Air-conditioning	Refrigeration
N_z	–	12/8/6	Solution mass flow	(kg/s)	0.00178–0.45677	
N_y	–	2/3/4	Vapour mass flow	(kg/s)	0.00050–0.12800	
Distance between tubes, x direction	(m)	31.7×10^{-3}	Air mass flow	(kg/s)	0.214–0.858	
Distance between tubes, y direction	(m)	27.5×10^{-3}	Solution temperature	(°C)	87.8	57.4
Tube, outer diameter	(m)	12.7×10^{-3}	Vapour temperature	(°C)	1.1	−30.6
Tube, thickness	(m)	0.9×10^{-3}	Air temperature	(°C)	43.3	30.0
Vapour injector holes diameter (*)	(m)	1.0×10^{-3}	Solution concentration	(%w NH_3)	24.0	7.0
L_x	(m)	380.0×10^{-3}	Vapour concentration	(%w NH_3)	99.9	99.0
Fin pitch	(m)	2.0×10^{-3}	Pressure	(kPa)	448.0	116.8

* Only in bubble mode.

(a)

(b)
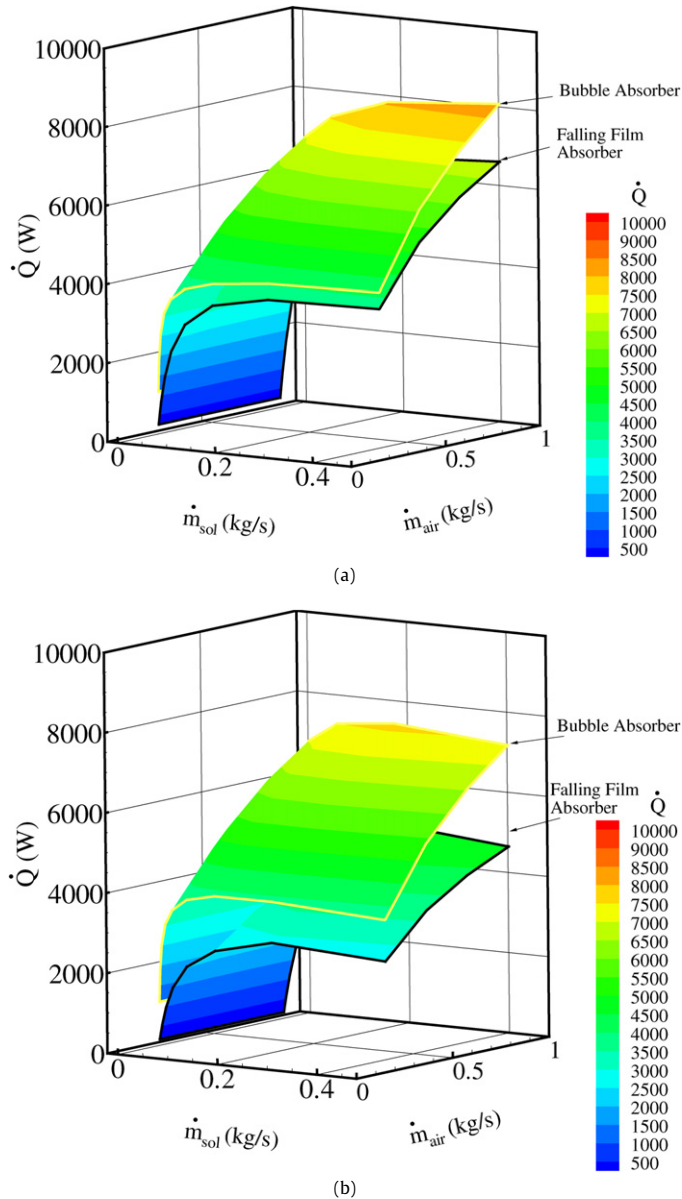
Fig. 8. Heat dissipated of the absorber vs. mass flow of air and solution (2×12 tube arrangement, air-conditioning (a) and refrigeration (b) conditions).

critical value is reached earlier in bubble than in falling film regime.

Under bubbly flow, the absorber is more efficient than in falling film flow in the regimes studied. This advantage is really important when the solution mass flow is small (low capacity applications),

and there is a low wetted area, therefore the useful area for heat and mass transfer is really low. Only falling film absorbers are competitive (with a difference only about 10%) close to the minimum flow that assures a complete wetted area. At higher solution flow regimes, the difference between the bubble and falling film absorber increases again favourably to the bubble flow one, but it has to be pointed out that the model developed for falling film flow does not take into account the possible heat and mass transfer enhancements due to the appearance of waves in the falling film. Moreover, the possible influence of pressure drop in the injection of the vapour in bubble regime is not considered.

The wetted area of the tubes versus the solution mass flow is demonstrated in Fig. 10 for the falling film regime. The variation is almost linear, until the 100% is reached at a mass flow of 0.2 kg/s, that corresponds to a falling film Reynolds number of approximately 2600.

4.2. Influence of the tube arrangement

Fig. 11 depicts the calculated air pressure drop vs. the air mass flow for the three type of absorbers according the tube arrangement. The relation between the pressure drop and the air mass flow is approximately quadratic: $\Delta p \cong K\dot{m}^n$, where $K = 139.8$ and $n = 1.69$ for the 2×12 absorber, $K = 411.6$ and $n = 1.72$ for the 3×8, and $K = 854.1$ and $n = 1.71$ for the 4×6 (Δp in Pa and $\dot{m}$ in kg s^{-1}). The arrangement of 2 rows $\times$ 12 columns is clearly preferred for applications where the forced convection is induced by an axial fan. The other two options (3 rows $\times$ 8 columns and 4 rows $\times$ 6 columns) are only attractive in cases where higher pressure drops are acceptable [28].

If the performance of the three type of absorbers are compared, there are not important differences between them from a qualitative point of view (Figs. 8 and 12) in relative terms for bubble and falling film flow, and under both air-conditioning and refrigeration conditions.

From a quantitative point of view, there are higher values of heat dissipated for the absorbers of arrangements with more tubes in air flow direction. This result is logical taking into account that more tubes in air flow direction implies a lower face area, therefore the air velocity is higher for the same mass flow and, consequently, the heat transfer coefficients in the air side.

5. Conclusions

The conclusions of the work can be summarised in the following items:

- There is a good agreement between the prediction of the heat rejected by the models developed and the experimental results for falling film absorption.
- In falling film absorption, the model overpredicts the change of concentration and underpredicts the change of tempera-
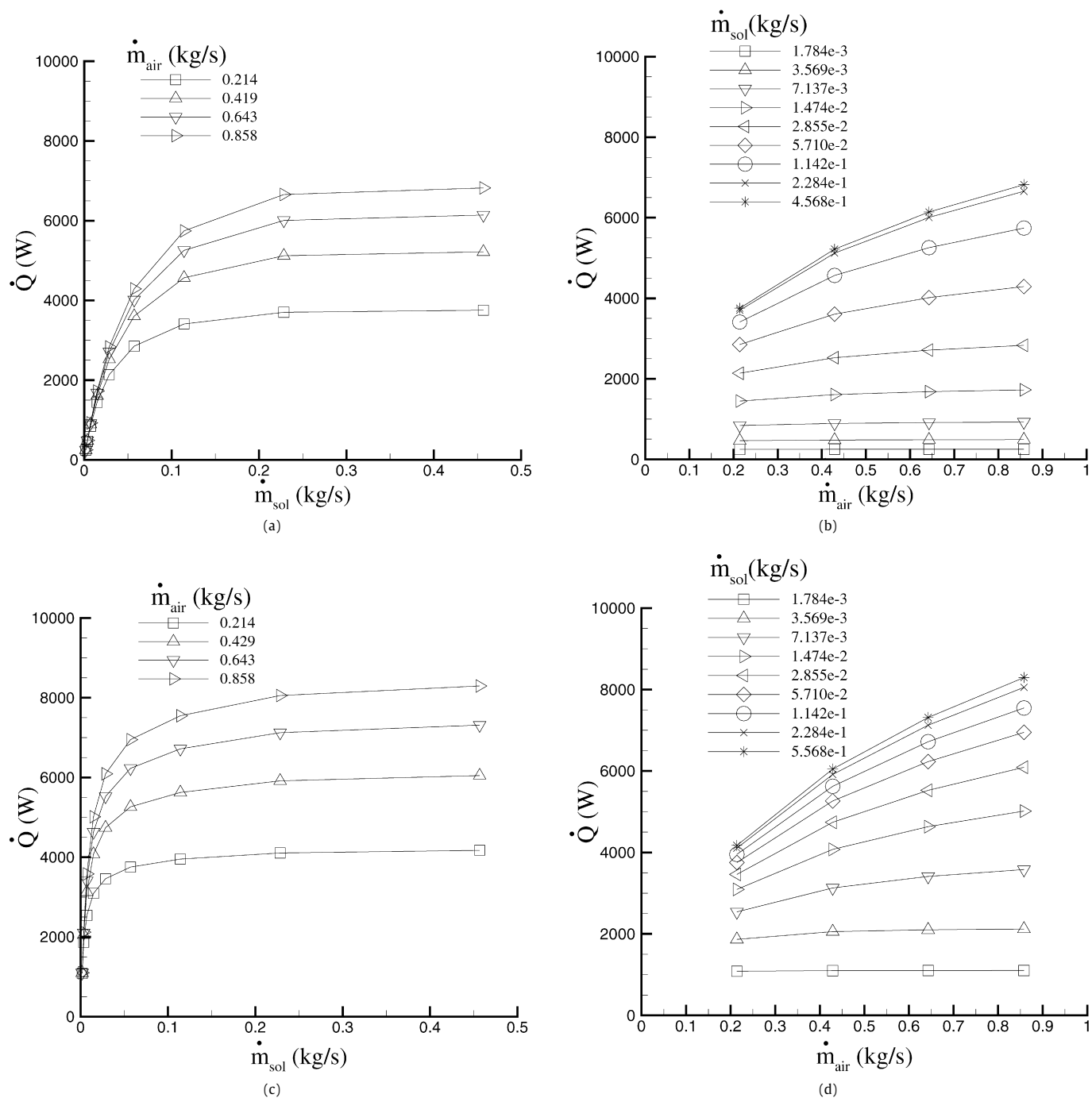
Fig. 9. Heat dissipated vs. different mass flows: (a) solution, falling film flow, (b) air, falling film flow, (c) solution, bubble flow, (d) air, bubble flow (2×12 tube arrangement, air-conditioning conditions).

ture. One of the reasons could be the difference of the two-dimensional velocity field considered in the falling film calculation, and the real three-dimensional one of the rivulets produced in the incomplete wettability of the tube.

- In bubble absorption there are some discrepancies of the profiles of mass absorbed of ammonia and water with respect to the model proposed by Herbine and Pérez-Blanco [13]. These discrepancies can be explained due to differences between the two models.

- Bubble absorption is in general more efficient than falling film absorption, specially for low solution flow rates. This fact is explained for the low wetted area in falling film flow under such regimes. These low solution flow rates are more characteris-

tic for absorbers of low capacity. Therefore, the bubble flow is more suitable in such applications. However, the difference is relatively small (about 10%) close to the minimum solution falling film flow with a complete area wetted.

- There is not significant differences from a qualitative point of view between air-conditioning or refrigeration applications.

- The three different tube arrangements produce similar qualitative results. The only difference is an increase of the heat dissipated due to the increment of the air velocity and, by consequence, of the heat transfer coefficients for the arrangements with more tubes in air direction (3×8 and 4×6). However, these arrangements produce an important increase of the air pressure drop.
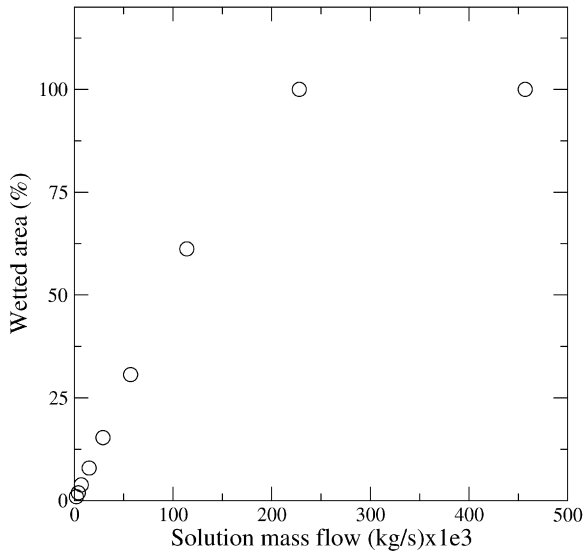
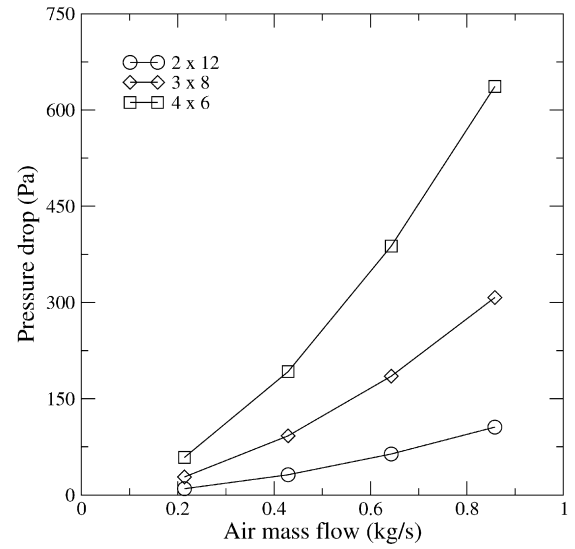**Fig. 10.** Wetted area versus the solution mass flows.

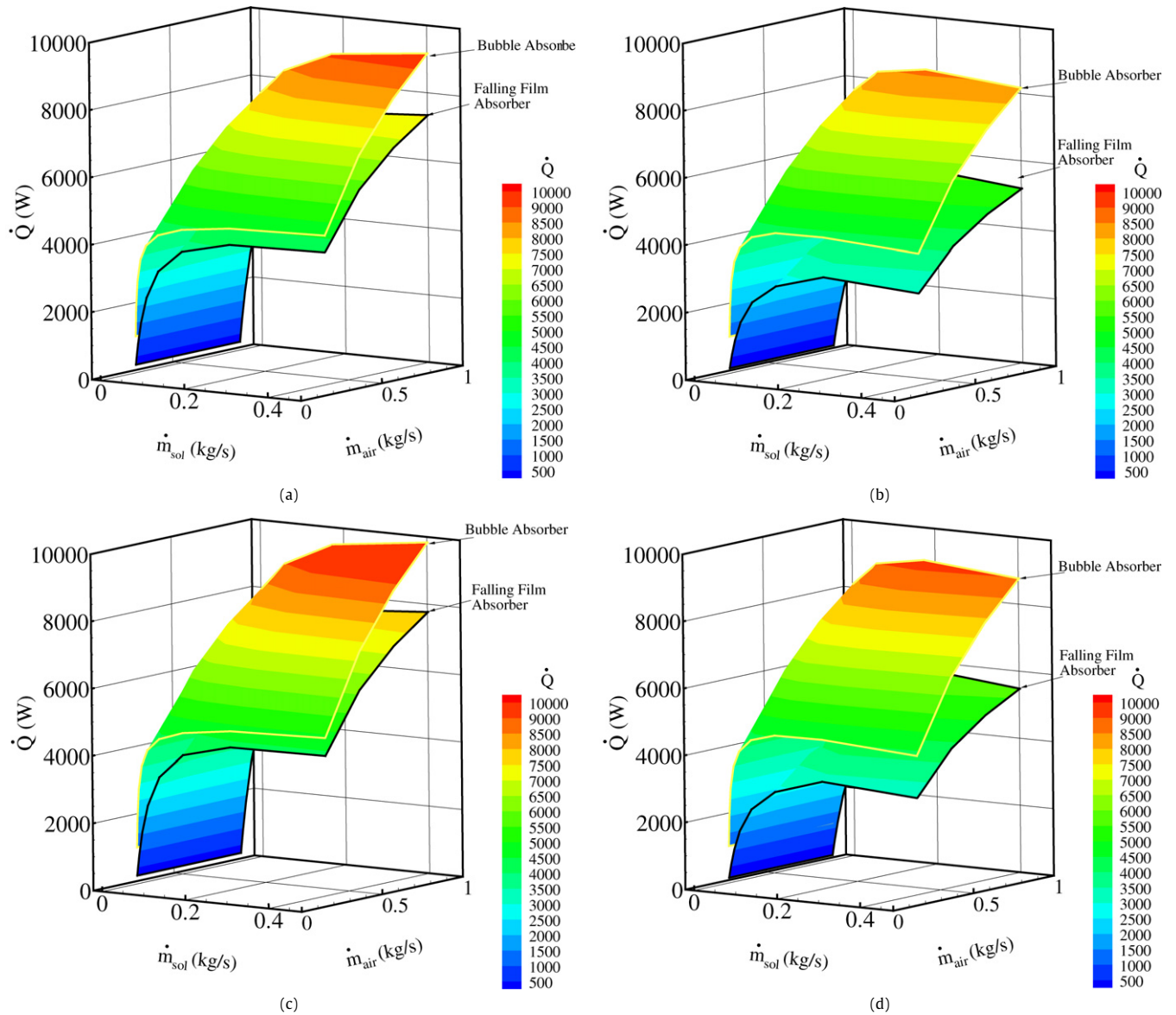**Fig. 11.** Pressure drop for the different heat exchanger tube arrangements.

Fig. 12. Heat dissipated of the absorber vs. mass flow of air and solution for: (a) 3×8 tube arrangement, air-conditioning, (b) 3×8 tube arrangement, refrigeration, (c) 4×6 tube arrangement, air-conditioning, (d) 4×6 tube arrangement, refrigeration.

References

[1] J. Castro, A. Oliva, C.D. Pérez-Segarra, J. Cadafalch, Evaluation of a small capacity, hot water driven, air-cooled H_2O–LiBr absorption machine, International Journal of Heat Ventilation Air Conditioning and Refrigeration Research 13 (1) (2007) 59–75.

[2] D.C. Erickson, Extending the boundaries of ammonia absorption chillers, ASHRAE Journal 49 (4) (2007) 32–35.

[3] B. Agnewa, M. Talbi, M. Mostafavi, Combined power and cooling, an analysis of the combined diesel-absorption cycle, Applied Thermal Engineering 19 (10) (1999) 1097–1105.

[4] G.A. Longo, A. Gasparella, C. Zilio, Analysis of an absorption machine driven by the heat recovery on an I.C. reciprocating engine, International Journal of Energy Research 29 (8) (2005) 711–722.

[5] M. Salim, Technical potential for thermally driven mobile A/C systems, SAE Technical Paper Series (2001-01-0297), 2001, pp. 1–12.

[6] I. Horuz, An alternative road transport refrigeration, Turkish Journal of Engineering and Environmental Science 22 (1998) 211–222.

[7] J. Koehler, W.J. Tegethoff, D. Westphalen, M. Sonnekalb, Absorption refrigeration system for mobile applications utilizing exhaust gases, Heat and Mass Transfer 32 (5) (1997) 333–340.

[8] J. Fernández-Seara, A. Vales, M. Vázquez, Heat recovery system to power an on-board NH_3–H_2O absorption refrigeration plant in trawler chiller fishing vessels, Applied Thermal Engineering 18 (12) (1998) 1189–1205.

[9] H. Pérez-Blanco, A model of an ammonia–water falling film absorber, ASHRAE Transactions 94 (1) (1988) 467–483.

[10] C.C. Mihaila, F.N. Chiriac, I.D. Sota, F.I. Baltaretu, The modelling of a film absorber with ammonia–water solution, in: Proceedings of the 19th International Congress of Refrigeration, 1995, pp. 154–160.

[11] B. Kim, Heat and mass transfer in a falling film absorber of ammonia–water absorption systems, Heat Transfer Engineering 19 (3) (1998) 53–63.

[12] K. Gommed, G. Grossman, M. Koenig, Numerical study of absorption in a laminar falling film of ammonia–water, ASHRAE Transactions 107 (1) (2001) 453–462.

[13] G.S. Herbine, H. Pérez-Blanco, A model of an ammonia–water bubble absorber, ASHRAE Transactions 101 (1) (1995) 1324–1331.

[14] J.C. Lee, K.B. Lee, B.H. Chun, C.H. Lee, J.J. Ha, S.H. Kim, A study on numerical simulations and experiments for mass transfer in bubble mode absorber of ammonia and water, International Journal of Refrigeration 26 (5) (2003) 551–558.

[15] T.Y. Kang, A. Akisawa, T. Kashiwagi, Analytical investigation of two different absorption modes: Falling film and bubble types, International Journal of Refrigeration 23 (6) (2000) 430–443.

[16] C. Oliet, C.D. PTrez-Segarra, S. Danov, A. Oliva, Numerical simulation of dehumidifying fin-and-tube heat exchangers. Model strategies and experimental comparisons, in: Proceedings of the 2002 International Refrigeration Engineering Conference at Purdue, 2002, pp. 1–8.

[17] C.D. Pérez-Segarra, C. Oliet, A. Oliva, Thermal and fluid dynamic simulation of automotive fin-and-tube heat exchangers. Part 1: Mathematical model, Heat Transfer Engineering 29 (5) (2008) 484–494.

[18] C. Oliet, C.D. Pérez-Segarra, A. Oliva, Thermal and fluid dynamic simulation of automotive fin-and-tube heat exchangers. Part 2: Experimental comparison, Heat Transfer Engineering 29 (5) (2008) 495–502.

[19] N.H. Kim, J.H. Yun, R.L. Webb, Heat transfer and friction correlations for wavy plate fin-and-tube heat exchangers, Journal of Heat Transfer – Transactions of ASME 119 (3) (1997) 560–567.

[20] J. Castro, L. Leal, P. Pozo, A. Oliva, Performance of an air-cooled, falling film absorber of an ammonia–water absorption cooling machine, in: Proceedings of the 3rd International Symposium on Two-Phase Modelling and Experimentation, 2004, pp. 2193–2199.

[21] J. Castro, A. Oliva, C.D. Pérez-Segarra, C. Oliet, Modelling of the heat exchangers of a small capacity, hot water driven, air-cooled H_2O–LiBr absorption cooling machine, International Journal of Refrigeration 31 (1) (2008) 75–86.

[22] R.B. Bird, E.E. Stewart, E.N. Lightfoot, Transport Phenomena, John Wiley and Sons Inc., 1960.

[23] J. Andberg, Absorption of vapours into liquid films flowing over cooled horizontal tubes, PhD thesis, University of Texas, 1986.

[24] J. Patek, J. Klomfar, Simple functions for fast calculations of selected thermodynamic properties of the ammonia–water system, International Journal of Refrigeration 18 (4) (1995) 228–234.

[25] J. Mikielewicz, J.R. Moszynski, Minimum thickness of a liquid film flowing vertically down a solid surface, International Journal of Heat and Mass Transfer 19 (7) (1976) 771–776.

[26] J. Castro, C. Oliet, J. Farnós, A. Oliva, Numerical study of falling film and bubble absorbers for small capacity NH_3–H_2O air-cooled absorption systems, in: Proceedings of the 22th International Congress of Refrigeration, 2007, pp. 1–8.

[27] R.E. Treybal, Mass Transfer Operations, McGraw-Hill, 1980.

[28] V. Mei, S.K. Chaturvedi, B. Zalmen Lavan, A truck exhaust gas operated absorption refrigeration system, ASHRAE Transactions B (2531) (1982) 66–76.